https://doi.org/10.5194/egusphere-2026-1366
Preprint. Discussion started: 20 April 2026

Freshwater sources and circulation in northern Greenland fjords from a multi-tracer analysis

Camille Hayatte Akhoudas[1,2*], Johan Nilsson[3], William Jenkins[4], Jamie Barnett[1,2], Jürgen Sültenfuß[5], Nina Kirchner[6], Martin Jakobsson[1,2], and Christian Stranne[1,2]

[1]Department of Geological Sciences, Stockholm University, Stockholm, Sweden
[2]Bolin Centre for Climate Research, Stockholm University, Stockholm, Sweden
[3]Department of Meteorology, Stockholm University, Stockholm, Sweden
[4]Department of Marine Chemistry and Geochemistry, Woods Hole Oceanographic Institution, Woods Hole MA, 02543 United States
[5]Institute of Environmental Physics, University of Bremen, Bremen, Germany
[6]Department of Physical Geography, Stockholm University, Stockholm, Sweden

Correspondence: Camille Hayatte Akhoudas (camille.akhoudas@geo.su.se)

Abstract.

Northern Greenland fjords regulate the interaction between the ocean and two major marine-terminating glaciers, yet the sources and pathways of freshwater that transform fjord waters remain incompletely understood. During the *GEOEO-North of Greenland 2024 Expedition*, hydrographic observations together with water oxygen isotopes (δ^{18}O) and noble gas tracers (helium and neon) were collected in Petermann and Victoria fjords to characterize water-mass and freshwater composition and to identify glacial meltwater pathways during late summer. The observations reveal pronounced differences between the two fjords; Petermann Fjord exhibited a relatively well-mixed surface layer under largely ice-free conditions, consistent with active ventilation and exchange with shelf waters, and in contrast, Victoria Fjord retained a shallow and strongly stratified surface layer beneath persistent sea-ice and dense iceberg mélange, conditions that likely limited air-sea exchange and enhanced freshwater accumulation in the upper layer. The combined hydrographic, isotope, and tracer framework indicates that freshwater in the upper layer of both fjords was dominated by meteoric input mainly derived from local glacial melt, while contributions from Arctic-sourced freshwater were comparatively small. Noble gas anomalies further identify glacially modified waters below the mixed layer, revealing a subsurface layer influenced by meltwater between roughly 100 and 250 m depth. Tracer distributions suggest that meltwater enters the fjords through multiple pathways, including subglacial discharge that influences the upper water column, and submarine melting that affects deeper layers by mixing with Atlantic-origin waters. These observations provide new constraints on meltwater pathways and circulation in northern Greenland fjords and help elucidate how ocean forcing can influence ice–ocean interactions in this rapidly changing region.

1 Introduction

The fjords along the northern margin of Greenland form critical interfaces between the ice-sheet and the ocean, regulating exchanges of heat and freshwater that influence glacier dynamics, regional circulation, and ultimately Greenland's contribu-

https://doi.org/10.5194/egusphere-2026-1366
Preprint. Discussion started: 20 April 2026

tion to sea-level rise (Straneo and Cenedese, 2015). Over recent decades, this region has undergone substantial change: after remaining close to mass balance during the early 1970s, the northern drainage sector of the Greenland Ice Sheet (Fig. 1a) has experienced sustained mass loss of roughly 50 Gt yr^{-1}, continuing into the early 2020s and projected to persist under future warming models (Pattyn et al., 2018; Mouginot et al., 2019; Otosaka et al., 2022; Greve and Chambers, 2022). This loss reflects the combined effects of increased surface melt and runoff, enhanced subglacial discharge, and intensified submarine melting at marine-terminating glaciers (Enderlin et al., 2014; Mouginot et al., 2019; Slater and Straneo, 2022). Concurrently, floating ice tongues along the northern coast have thinned substantially, losing more than 35 % of their volume since 1978, with accelerated thinning since 2000 coincident with warming of deep ocean waters (Millan et al., 2023). Together, these observations highlight the growing importance of ice–ocean interactions in shaping the evolution of northern Greenland glaciers. A key control on these interactions is the structure of the fjords themselves. Fjord bathymetry and geometry regulate the access of ocean waters to glacier fronts and therefore influence the delivery of oceanic heat capable of driving submarine melting (Jakobsson et al., 2020; Nilsson et al., 2023; Schaffer et al., 2020). In northern Greenland fjords, relatively warm and saline Atlantic waters occupy deeper layers beneath colder and fresher Polar waters, forming the dominant water-mass structure of the fjord environment (Fig. 1b). Whether warm deep waters can flow toward glacier fronts strongly depends on bathymetric features such as sills and troughs, which can either permit or restrict inflow. These controls make fjords central in determining how glaciers respond to oceanic forcing, although large-scale hydrographic variability also influence the accessibility of Atlantic waters to fjords, as shown on the Northeast Greenland shelf (Gjelstrup et al., 2022). Within fjords, ocean circulation is further shaped by the interaction between freshwater input and the surrounding ambient waters. Submarine melting (ocean-driven melting of the submerged ice front) and subglacial discharge (meltwater from the glacier surface, routed through subglacial drainage systems and emerging at the ice front) generate buoyant plumes that entrain ambient fjord waters as they rise (Jenkins, 2011; Carroll et al., 2015; Slater et al., 2015; Wekerle et al., 2024; Wiskandt et al., 2025). Through this process, mixtures of meltwater and entrained fjord water, commonly referred to as glacially modified waters, are produced (Fig. 1b) and play a major role in driving fjord circulation and regulating freshwater export to the continental shelf (Straneo and Cenedese, 2015; Cowton et al., 2015; Muilwijk et al., 2022; Vries et al., 2025; Wekerle et al., 2024). Consequently, fjord processes not only regulate local ice–ocean interactions but may also influence the stratification and circulation of the broader Arctic Ocean. Despite their importance, northern Greenland fjords remain among the least observed in the Arctic. Their remote location and extensive sea-ice cover have limited direct measurements, and their complex geometry and bathymetry are only recently becoming better resolved (Jakobsson et al., 2024). As a result, the composition, transformation, and pathways of freshwater exported from these systems remain poorly constrained. Numerical models have begun to explore the impact of freshwater discharge from northern Greenland (Prakash et al., 2025; Wekerle et al., 2024), yet most simulations operate at spatial resolutions that are too coarse to adequately represent fjord-scale circulation and ice–ocean interactions. This limitation often leads to simplified freshwater distributions and an incomplete representation of the processes that form glacially modified water (Dukhovskoy et al., 2016). Improved observational constraints are therefore needed to better understand how freshwater is distributed and transformed within northern Greenland fjord systems.

https://doi.org/10.5194/egusphere-2026-1366
Preprint. Discussion started: 20 April 2026

Distinguishing the sources of freshwater within fjords is challenging when relying on hydrographic properties alone, as salinity and temperature cannot uniquely separate meteoric freshwater derived from precipitation, runoff, glacial meltwater, or freshwater associated with sea-ice processes. Stable water isotopes, used in tandem with hydrographic properties, provide a powerful tool for differentiating these freshwater end-members because meteoric water and sea-ice melt exhibit distinct isotopic signatures that reflect their formation processes (Bauch et al., 1995, 2005; Charette et al., 2020; Kopec et al., 2024). Furthermore, when combined with noble gases and their isotopes, this integrated tracer approach enables the identification of glacial inputs within the meteoric water pool particularly through the distinct signatures acquired during ice–ocean interaction (Schlosser, 1986; Loose and Jenkins, 2014; Beaird et al., 2015, 2018; Huhn et al., 2021). Here we apply this multi-tracer framework to Petermann and Victoria fjords in northwest Greenland, two neighboring systems that experience similar offshore forcing but differ in geometry, bathymetry, and glacier configuration (Jakobsson et al., in review). Petermann Fjord hosts one of the last remaining large floating ice tongues in the Northern Hemisphere, while Victoria Fjord is fed by C.H. Ostenfeld Gletsjer, which largely terminates at the grounding line. These contrasting settings provide a natural laboratory for investigating how fjord characteristics and glacier type influence freshwater distribution and transformation. Observations were collected during the *GEOEO-North of Greenland 2024 Expedition* (hereafter *GEOEO 2024*) onboard the Swedish icebreaker *Oden*, including the first marine measurements from Victoria Fjord (Jakobsson et al., in review). This study addresses three main questions: (1) what are the dominant freshwater sources in Petermann and Victoria fjords, (2) how do their distributions differ between the two systems, and (3) whether tracer signatures reveal characteristic water-mass structures associated with glacially modified waters. By combining hydrographic, isotopic, and noble-gas observations, we aim to better constrain a poorly observed pathway through which glacier–fjord processes further influence the stratification and circulation of the Arctic Ocean.

2 Regional setting

Northwest Greenland occupies a key oceanographic gateway between the Arctic Ocean and Baffin Bay through the Nares Strait (Fig. 1a,c). This narrow passage, approximately 500 km long and about 40 km wide, contains a sill of roughly 220 m depth between Smith Sound and Kennedy Channel (Jakobsson et al., 2024). The geometry of the strait regulates the exchange of heat and freshwater between the Arctic and the North Atlantic and therefore influences the hydrographic properties of waters reaching the fjords along the northwestern Greenland margin. North of the strait lies the Lincoln Sea, one of the least observed regions of the Arctic Ocean, where hydrographic measurements remain sparse and multiyear sea-ice persists for much of the year (Moore et al., 2019). Variability in sea-ice dynamics across the Lincoln Sea–Nares Strait system affects freshwater storage, upper-ocean stratification, and the timing of seasonal sea-ice breakup in adjacent fjords (Washam et al., 2018; Stranne et al., 2021). Consequently, the oceanographic conditions within these fjords are closely linked to processes across this broader Arctic gateway.

Among the fjords connected to this system, Petermann Fjord hosts Petermann Gletsjer, one of the largest marine-terminating glaciers in Greenland, draining approximately 8.5 % of the Greenland Ice Sheet (Hill et al., 2017). Until 2010, the glacier supported a floating ice tongue extending about 60 km into the fjord, which experienced major calving events in 2010 and

https://doi.org/10.5194/egusphere-2026-1366
Preprint. Discussion started: 20 April 2026

2012 that substantially reduced its extent (Falkner et al., 2011; Münchow et al., 2014). Subsequent studies documented episodic intrusions of relatively warm deep waters into the fjord and beneath the remaining ice tongue, emphasizing the sensitivity of the glacier–fjord system to oceanic forcing (Johnson et al., 2011; Heuzé et al., 2017; Washam et al., 2018; Jakobsson et al., 2020). Consistent with many glacial fjords, circulation in Petermann Fjord exhibits an estuarine-like structure, with a buoyant outflow enriched in meltwater occupying the upper layer and a compensating inflow of deeper shelf-derived waters entering the fjord interior (Münchow, 2016; Heuzé et al., 2017).

Victoria Fjord, located north of Petermann Fjord and connected to the southern part of the Lincoln Sea, provides an important contrasting system. It is fed primarily by C.H. Ostenfeld Gletsjer, which previously supported a floating ice tongue that rapidly disintegrated in the early 2000s (Hill et al., 2017). Following this collapse, the glacier now terminates at a grounded ice-cliff, and the inner fjord is commonly filled with dense ice mélange and large icebergs. Compared with Petermann Fjord, Victoria Fjord is generally characterized by more extensive and persistent sea-ice cover, reflecting both its geographic setting and the limited exchange with shelf waters. Direct oceanographic observations from the fjord have historically been absent; however, scarce open-water area during the summer of 2024 allowed the first hydrographic measurements to be collected there, providing initial constraints on the oceanographic structure of this previously unsampled system (Jakobsson et al., in review).

3 Data and Methods

3.1 Observations

The *GEOEO 2024* was carried out between 6 August and 17 September 2024 in northern Greenland. Oceanographic profiles of temperature and salinity were acquired using a Seabird 911+ CTD system. The instrument was lowered at a rate of ∼0.5 m s^{-1} and stopped approximately 10 m above the seafloor, guided by an altimeter mounted on the rosette frame. Temperature and salinity values are further reported as conservative temperature (Θ) and absolute salinity (S_A), following TEOS-10. A total of 120 water samples were collected from 15 stations for measurements of noble gas concentration and their isotopes (^{3}He, ^{4}He, ^{20}Ne), water oxygen isotopes (δ^{18}O), and tritium (^{3}H) in Victoria and Petermann fjords as well as a station control in the Lincoln Sea (Fig. 1c). The water samples for He and Ne were collected from the Niskin bottles immediately after CTD recovery using gas-tight copper tubes and in 1L plastic bottles for ^{3}H, and subsequently analyzed in the Helis noble gas mass spectrometry laboratory (Sültenfuß et al., 2009) at the University of Bremen. Ultimately, 97 valid measurements were obtained. Based on replicate samples, the uncertainty for He and Ne concentrations, ^{3}He/^{4}He ratio and ^{3}H were determined to be ± 0.5 %, ± 0.4 % and ± 3 %, respectively. δ^{18}O samples were drawn from the Niskin bottles into 2 ml glass vials and kept cool at 4 °C until further analysis in the Department of Geological Sciences of Stockholm University using a Picarro L2140–I analyzer (cavity ring-down spectrometer; CRDS). The obtained isotopic compositions were expressed as δ notation with reference to standards: $\delta = \left(\frac{R_{\text{sample}}}{R_{\text{standard}}} - 1\right) \times 1000‰$, where R is the ratio of heavy to light oxygen isotopes, ^{18}O and ^{16}O, respectively. The standards used were the Vienna Standard Modern Ocean Water (VSMOW) and 3 internal standards. The precision is 0.02 ‰ for δ^{18}O by CRDS measurement; however, seawater samples are analyzed directly by the CRDS using a stain-free liner from

https://doi.org/10.5194/egusphere-2026-1366
Preprint. Discussion started: 20 April 2026

Picarro Inc. that is inserted into the injection port to avoid salt accumulation in the vaporizer. The mesh traps about 80 % of the salt (Benetti et al., 2017) and then the final precision is estimated to be 0.06 ‰.

3.2 Water-mass definitions

To obtain greater insight into the hydrographic structure of Petermann and Victoria fjords, we distinguish between oceanic water-masses and freshwater following previous studies of fjords in northwestern Greenland (e.g., Johnson et al., 2011; Jakobsson et al., 2020; Stranne et al., 2021; Münchow, 2016; Shroyer et al., 2017; Münchow et al., 2014; Washam et al., 2018). Therefore, we assume that two main oceanic water-masses dominate the vertical structure: cold and relatively fresh Polar Water (PW) overlying warm and saline Atlantic Water (AW). PW is characterized by relatively low temperature and salinity and originates from the surface layer of the Arctic Ocean. Beneath this layer, AW is distinguished by higher temperature and salinity and enters the Arctic Ocean primarily through the Fram Strait and the Barents Sea before circulating toward northern Greenland.

Within this hydrographic framework, the freshwater content can be further divided into different sources. We distinguish meteoric water (MW), which includes freshwater derived from precipitation, glacial melt, Arctic rivers, and terrestrial runoff, from sea-ice melt (SIM), which represents freshwater released during the melting of sea-ice. Freshwater derived from glacial melt is therefore included within this broad MW pool but, to better resolve its contribution, it is further decomposed into three components with distinct formation mechanisms and tracer signatures. The first component is subglacial discharge (SGD), composed of meltwater produced at the ice-sheet surface that drains through the subglacial hydrological system and is released at the glacier front. The second component is submarine meltwater (SMW), which forms directly at the subsurface ice–ocean interface as a result of oceanic heat flux. A third component, ancient ice melt (AIM), represents meltwater derived from older glacial ice that has accumulated radiogenic helium during prolonged residence near the bedrock. Although AIM originates from processes similar to those producing SMW or SGD, it is geochemically distinct due to enrichment in crustal ^{4}He and modified ^{3}He/^{4}He ratios. Finally, the remaining fraction of the MW pool represents freshwater derived from precipitation, Arctic rivers, and terrestrial runoff.

3.3 Noble gases and δ^{18}O as conservative tracers

To quantify freshwater and oceanic contributions, we apply a δ^{18}O–S_A mass balance together with an Optimum Multiparameter (OMP) analysis. These two approaches provide complementary constraints: the δ^{18}O–S_A framework distinguishes meteoric water (MW) from sea-ice melt (SIM), while the inclusion of noble gas tracers in the OMP analysis allows further resolution of different glacial meltwater components (i.e., SGD, SMW and AIM) within the MW pool and, in addition, oceanic source waters (AW and PW). These methods rely on the contrasting geochemical and physical properties of the different end-members.

Because meteoric waters are strongly depleted in ^{18}O, with values reaching –30 ‰ (Masson-Delmotte et al., 2008), δ^{18}O is a robust tracer of freshwater inputs to polar oceans (Weiss et al., 1979; Östlund and Hut, 1984; Yamamoto-Kawai et al., 2005). In contrast, sea-ice formation and melt strongly modify salinity but produce only limited isotopic fractionation (1.5–2.7 ‰;

https://doi.org/10.5194/egusphere-2026-1366
Preprint. Discussion started: 20 April 2026

Ekwurzel et al., 2001; Song et al., 2025). Therefore, the combined use of salinity and δ^{18}O enables the separation of meteoric water and sea-ice contributions within a three end-member mass balance following Östlund and Hut (1984):

$$\begin{cases} 1 = f_{AW} + f_{SIM} + f_{MW} \\ S_{obs} = f_{AW} \cdot S_{AW} + f_{SIM} \cdot S_{SIM} + f_{MW} \cdot S_{MW} \\ \delta^{18}O_{obs} = f_{AW} \cdot \delta^{18}O_{AW} + f_{SIM} \cdot \delta^{18}O_{SIM} + f_{MW} \cdot \delta^{18}O_{MW} \end{cases}, \quad (1)$$

where f_{AW}, f_{SIM}, and f_{MW} represent the fractions of Atlantic Water, sea-ice melt and meteoric water, respectively. The system is solved using observed salinity and δ^{18}O values and defined end-member properties shown in Table 1. AW characteristics were identified in Θ–S_A space (Fig. 1d). MW is defined by S = 0 and δ^{18}O = –28 $\pm$ 4 ‰, and SIM by S = 4 and δ^{18}O = –4 $\pm$ 3 ‰. Negative f_{SIM} values indicate net sea-ice formation.

To further distinguish the glacial meltwater components in the MW pool, we use noble gases; helium (He) and neon (Ne) as conservative tracers. These gases are weakly soluble in seawater (Loose and Jenkins, 2014); while glacial ice contains atmospheric air trapped as bubbles during the transformation from snow to ice. When this ice melts under high hydrostatic pressure, the gases dissolve completely, producing substantial He and Ne excesses. Consequently, pure glacial meltwater may exhibit He and Ne concentrations up to 1280 % and 890 % above equilibrium, respectively (Loose and Jenkins, 2014). These large excesses allow detection of glacial meltwater fractions as low as ~0.05 % (Huhn et al., 2008; Sültenfuß et al., 2009). Gas excess, i.e., ΔHe and ΔNe, is expressed as:

$$\Delta C = \left(\frac{C_{sample}}{C_{sat}} - 1 \right) \times 100\%, \quad (2)$$

where C_{sample} is the measured He or Ne concentration and C_{sat} the solubility equilibrium concentration at *in situ* temperature and salinity (Jenkins et al., 2019). To further constrain the origin of He, we additionally use $\delta^3\mathrm{He} = \left(\frac{(^3\mathrm{He}/^4\mathrm{He})_{\mathrm{sample}}}{(^3\mathrm{He}/^4\mathrm{He})_{\mathrm{standard}}} - 1 \right) \times 100\%$, which allows us to distinguish between atmospheric and crustal He contributions. Radiogenic ^{4}He produced within the crust may accumulate in basal ice and be released during melting (Craig and Scarsi, 1997; Jean-Baptiste et al., 2001). As a result, such inputs increase the He/Ne ratios and lower the ^{3}He/^{4}He ratios relative to atmospheric values, a signal previously observed in Greenland fjords (Beaird et al., 2015, 2018; Huhn et al., 2021).

To isolate glacial meltwater contributions, the natural background saturation of noble gases associated with bubble injection and wave breaking must first be taken into account. At a deep reference site in the Lincoln Sea (>300 m), saturations were ~2.7 % for Ne and ~2.0 % for He, consistent with previous estimates (Rhein et al., 2018; Huhn et al., 2021). These background levels represent the regional baseline for noble gas content and are therefore subtracted from the observed ΔHe and ΔNe prior to further analysis. After correcting for this background signal, we estimate the relative contributions of oceanic and glacial source waters (AW, PW, SGD, SMW and AIM), using the OMP method following (Tomczak and Large, 1989). This approach assumes that the observed tracer properties result from conservative mixing among N source water types and determines their fractions by solving an overdetermined linear system subject to non-negativity and mass-conservation constraints. Prior to inversion, tracers were normalized using the mean and standard deviation of the source water matrix, following standard OMP

https://doi.org/10.5194/egusphere-2026-1366
Preprint. Discussion started: 20 April 2026

methodology:

$$\sum_{n=1}^{N} f_n T_{j,n} = T_j^{obs} + R_j \quad \text{for each tracer } j = 1, 2, \ldots, M, \tag{3}$$

with the additional constraint;

$$\sum_{n=1}^{N} f_n = 1, \tag{4}$$

where, f_n is the mixing fraction of source water type n, $T_{j,n}$ is the value of tracer j in source water type n, T_j^{obs} is the observed value of tracer j, R_j is the residual associated with tracer j, and M is the number of tracers (typically $M \geq N$). The tracers considered here are Θ, S_A, δ^{18}O, ^{3}He, He, and Ne.

In addition, the system is solved by minimizing the weighted sum of squared residuals:

$$\min_{f_n \geq 0} \left(\sum_{j=1}^{M} w_j^2 R_j^2 + w_{\text{mass}}^2 \left(\sum_{n=1}^{N} f_n - 1 \right)^2 \right), \tag{5}$$

Tracer weights w_j are defined to reflect the ability of each tracer to distinguish the source water types while accounting for measurement uncertainties:

$$w_j = \frac{\sigma_j^2}{\varepsilon_j^2}, \tag{6}$$

here, σ_j^2 is the variance of tracer j among the source water types (end-members), representing the ability of tracer j to separate the end-members, and ε_j^2 is the variance associated with the uncertainty of tracer j (measurement and end-member definition). This weighting scheme scales the tracer equations to a comparable dimensionless form while enhancing the influence of tracers that both vary strongly between end-members and are well constrained (Table 2).

To estimate the different water source fractions using this method, we first define the properties of the corresponding end-members (Table 1). The physical characteristics of AW and PW were determined from the Θ–S_A diagram (Fig. 1d). The associated He, Ne, and δ^{18}O values were then assigned from the observations located closest to each end-member in the Θ–S_A space. SGD was defined as meltwater that equilibrated with the atmosphere on the surface of the ice-sheet (S = 0 psu, T = 0 °C) and was subsequently isolated within the subglacial hydrological system (Beaird et al., 2018). Corresponding He and Ne concentrations were calculated from solubility equilibrium at S = 0 psu, T = 0 °C (Jenkins et al., 2019), representing atmospheric conditions at the time of formation. SMW, in contrast, forms through oceanic heat flux at the ice–ocean interface. The thermodynamic effect of melting is represented by an effective potential temperature of $\theta_{effSMW} = -87$°C (Loose et al., 2009), which accounts for sensible and latent heat requirements. Noble gas concentrations were estimated using the mean air content of Greenland ice cores (Martinerie et al., 1992) and assuming complete dissolution under hydrostatic pressure during melting; He = 26.4 nmol g^{-1}; Ne = 91.7 nmol g^{-1}. Finally, AIM represents meltwater enriched in radiogenic ^{4}He that accumulated during prolonged basal ice residence (Beaird et al., 2015, 2018; Huhn et al., 2021). This end-member is characterized by a depressed ^{3}He/^{4}He ratio (1.1×10^{-6}; ≈ 0.8 R$_A$) together with a elevated He/Ne ratio (2.25 × atmospheric;

https://doi.org/10.5194/egusphere-2026-1366
Preprint. Discussion started: 20 April 2026

$R_A \approx 1.38 \times 10^{-6}$; Clarke et al., 1976). These parameters were derived from the slope between background deep water conditions and the most He-enriched sample in our dataset, indicating the addition of a non-atmospheric He component.

3.4 Propagation of errors

The uncertainty in the source fractions derived from both the δ^{18}O–S_A mass balance and the OMP method was quantified using a Monte Carlo approach. For each observation, 10,000 perturbed realizations of tracer values were generated assuming normally distributed uncertainties based on analytical precision (Tables 1–2). Each realization was solved independently, yielding a distribution of source fractions. Uncertainty was estimated from the interquartile range of this distribution (25th to 75th percentiles), providing a robust measure of the spread associated with observational errors and the inversion procedure.

4 Results and Discussion

4.1 Vertical hydrographic and tracer structure

In Petermann Fjord, the upper 50 meters of the water column consisted of a well-mixed upper layer characterized by small vertical gradients in S_A and Θ, with S_A around 30 g kg^{-1} and Θ close to the freezing point (Fig. 2a–b). The absence of sea-ice during the survey period likely allowed more active air–sea exchange and greater wind-driven vertical mixing, facilitated by the wide entrance of the fjord into the Nares Strait (Johnson et al., 2011; Shroyer et al., 2017). Beneath the mixed layer, Petermann Fjord exhibited a typical hydrographic structure of the Greenland fjords, with a low-salinity Polar Water (PW) layer overlying a deep, warmer and more saline Atlantic Water (AW) layer. The 0°C isotherm defined the interface between these two layers at approximately 300 m, below which S_A and Θ increased to 34.95 g kg^{-1} and 0.38 °C, respectively (Fig. 2a–b). In contrast, Victoria Fjord showed a markedly different upper ocean structure. The late summer survey occurred under persistent, yet partial, openings, fast-ice cover with extensive iceberg fields, conditions that likely limited wind-driven mixing, air–sea exchange, and ventilation with the open ocean (Fraser et al., 2018; Cottier et al., 2010; Stranne et al., 2021). The seasonal sea-ice dynamic along the northern Greenland coast is highly localized and strongly influenced by wind forcing and open ocean sea-ice conditions (Moore et al., 2019, 2023). Therefore, compact pack ice in the Lincoln Sea may have restricted sea-ice export and delayed breakup, prolonging sea-ice cover within Victoria Fjord and trapping a dense iceberg mélange sourced from C.H. Ostenfeld Gletsjer. As a result, the upper fjord retained a very shallow and fresh surface layer, overlying a pronounced temperature minimum near 50 m depth (Fig. 2b). This structure is characteristic of stratified Greenland fjords where freshwater accumulates in the upper layer during summer, enhancing surface stratification (e.g., Sutherland et al., 2014; Beaird et al., 2018; Monteban et al., 2020; Stranne et al., 2021). Similar conditions have been documented in the nearby Sherard Osborn Fjord, where sea-ice damming at the entrance of the fjord maintains a strong surface pycnocline into late summer (Stranne et al., 2021). Together, these observations revealed a freshwater retention regime in Victoria Fjord in which sea-ice and iceberg cover limited horizontal and vertical mixing, allowing the accumulation of freshwater in the upper tens of meters.

https://doi.org/10.5194/egusphere-2026-1366
Preprint. Discussion started: 20 April 2026

This contrast in hydrographic structure was reflected in the vertical water oxygen isotope distributions (δ^{18}O, Fig. 2c). In Victoria Fjord, δ^{18}O values in the upper 50 m were strongly depleted, around 0.5 ‰ lighter than those observed in Petermann Fjord, indicating a greater influence of meteoric water. Below ∼50 m, both fjords exhibited a sharp transition toward more ^{18}O–enriched waters, with δ^{18}O increasing with depth and reaching maximum values below 300 m (Fig. 2c). However, significant differences emerged in the subsurface layer between ∼75 and 200 m. Waters in Victoria Fjord were warmer, saltier, and more enriched in ^{18}O than in Petermann Fjord (Fig. 2a–c). This likely reflects a stronger influence of AW and more efficient entrainment of the subsurface waters by glacially driven plumes, potentially modulated by the dense iceberg mélange observed in Victoria Fjord.

Vertical noble gas anomalies provide additional constraints on the contribution of glacially derived freshwater below the surface mixed layer (see Data and Methods). Elevated values of ΔHe and ΔNe were generally observed within the upper 300 m of both fjords (Fig. 2d–e), identifying subsurface layers enriched in glacial meltwater. In Victoria Fjord, ΔHe and ΔNe maxima occurred on a broad layer extending from 15 to 200 m, while in Petermann Fjord, the elevated values were restricted to a narrower depth range between ∼100 and 200 m. In addition, Victoria Fjord exhibited near-surface (15–50 m) ΔHe and ΔNe anomalies coinciding with strongly depleted δ^3He values, reaching –9 % (Fig. 2f) and indicative of enrichment in ^{4}He over ^{3}He as well as limited equilibration with the atmosphere. As mentioned above, the extensive sea-ice cover likely inhibited gas exchange, allowing near-surface waters to retain glacial meltwater characterized by an excess of He and Ne. In contrast, near-surface δ^3He values in Petermann Fjord remained close to the atmospheric equilibrium (∼–1.8 %; Fig. 2f), consistent with low ΔHe and ΔNe values likely due to more efficient ventilation and open-water conditions (Münchow et al., 2014; Johnson et al., 2011). Below 50 m depth, δ^3He values increased to approximately 7 % between 100 and 200 m in both fjords (Fig. 2f), coincident with subsurface elevated ΔHe and ΔNe values (Fig. 2d–e). These signatures are indicative of δ^3He-enriched, tritium-decayed (∼0.5 TU; Supplementary Fig. A1) Atlantic waters, which dominate the glacially modified layer commonly observed in Greenland fjords (e.g., Sutherland et al., 2014; Heuzé et al., 2017; Muilwijk et al., 2022; Rysgaard et al., 2024). At depths greater than ∼300 m, ΔHe and ΔNe stabilized within narrow ranges (ΔHe: 1–4 %; ΔNe: 2–4 %; Fig. 2d–e) and were associated with elevated δ^3He values of 10 % (Fig. 2f). This δ^3He excess reflects the time-integrated decay of largely nuclear weapons-produced tritium, consistent with the relatively old age of deep waters that enter the northwestern Greenland region (Pasqualini et al., 2024).

4.2 Tracer evidence for freshwater sources

Northern Greenland fjords receive freshwater from both local sources and the broader Arctic Ocean, the latter being exported through the Nares Strait (Burgers et al., 2023). This Arctic-derived freshwater is partly supplied by the Transpolar Drift, a major circulation pathway that transports surface waters and sea-ice across the Arctic Ocean toward the Greenland margin. Waters carried by this drift exhibit a characteristic oxygen isotope signature, with δ^{18}O values typically between –3 and –4 ‰ (Bauch et al., 2005). In addition to sea-ice–related freshwater, the Transpolar Drift can contain a substantial meteoric component derived from precipitation and runoff from major Arctic rivers. Estimates suggest that this meteoric contribution may account for up to ∼20 % of the transported freshwater, characterized by δ^{18}O end-member values of approximately –19

https://doi.org/10.5194/egusphere-2026-1366
Preprint. Discussion started: 20 April 2026

‰ (Charette et al., 2020). In both fjords, near-surface waters (above 100 m, corresponding to S_A < 33 g kg^{-1}) exhibited a strong relationship between δ^{18}O and S_A (solid blue line, Fig. 3a), indicating that the freshwater component in this layer is primarily meteoric in origin. Extrapolation of the mixing line to zero salinity yields a δ^{18}O intercept of –26 ± 3 ‰; an estimate more depleted than typical Arctic rivers but closely matches the isotopic composition of local glacial ice (–28 ± 4 ‰; Table 1). Together, these results indicate that meteoric freshwater in the upper layer was predominantly derived from local glacial melt, while contributions from Arctic-sourced freshwater transported into the region were comparatively small (Charette et al., 2020). In addition, the near-linear alignment of most observations along the δ^{18}O–S_A relationship suggests that mixing between freshwater and marine end-members was largely conservative, with only minor deviations likely reflecting sea-ice processes (i.e., formation and melt) but also measurement uncertainty. At depths below 100 m, waters in both fjords became saltier and occupied a narrower δ^{18}O–S_A range, a pattern consistent with the presence of inflowing Atlantic-derived waters that have mixed with locally modified fjord waters. A linear regression applied to observations between 100 and 300 m depth (solid red line, Fig. 3a) yields a freshwater end-member of –25 ± 1 ‰, which is indistinguishable from the estimate obtained for the upper 100 m (–26 ± 3 ‰). The similarity between these estimates indicates that, although the subsurface layer was primarily composed of Atlantic waters, its isotopic composition has been modified by mixing with glacially derived freshwater within the fjords.

Noble gas distributions provide an additional line of evidence for identifying glacial meltwater sources and tracing mixing processes within the fjords. The relationship between ^{3}He and ^{4}He revealed two distinct trends (Fig. 3b); observations from deep waters (>300 m) fell along a mixing line consistent with atmospheric He addition, characterized by a ^{3}He/^{4}He ratio of 1.38×10^{-6} (Clarke et al., 1976) and, in contrast, subsurface waters between 100 and 300 m deviated from this trend toward higher ^{4}He concentrations and lower ^{3}He/^{4}He ratios. This shift indicates reduced tritium-derived ^{3}He and suggests the presence of relatively young waters influenced by a non-atmospheric He source. An additional relationship emerged within the near-surface layer where observations defined a trend consistent with mixing between air-equilibrated seawater (AEW), representative of regional surface conditions (average temperature ≈ -1 °C and salinity ≈ 29.5 psu), and the highest He concentrations measured in Petermann Fjord (Fig. 3b). Near-surface observations from Petermann Fjord were largely plotted along this line, indicating that active gas exchange strongly influenced the upper ocean in this system. By contrast, near-surface observations from Victoria Fjord deviated from this trend toward lower ^{3}He/^{4}He ratios. This pattern reflects an enrichment in ^{4}He derived from a crustal source (Craig and Scarsi, 1997) and is consistent with previous observations of noble gas signatures in Greenland fjords that identify crustal He contributions associated with glacially modified waters (Beaird et al., 2015; Huhn et al., 2021). Because glacial meltwater is the only known source of concurrent He and Ne excesses in polar oceans (e.g., Schlosser, 1986; Hohmann et al., 2002; Hahm et al., 2004), anomalies in ΔHe and ΔNe can be used to directly estimate the contribution of glacial meltwater to fjord waters. Under the assumption that 1 % glacial ice is added to background seawater (green diamond, Fig. 3c), the resulting mixed water is expected to exhibit ΔHe ≈ 14.8 % and ΔNe ≈ 9.6 %. Observations from both fjords generally followed this predicted pure glacial meltwater mixing relationship (dashed green line, Fig. 3c), confirming that the measured noble gas anomalies primarily reflect glacial inputs. However, a subset of observations in both fjords exhibited elevated He relative to Ne, indicating the presence of an additional He source beyond that supplied

https://doi.org/10.5194/egusphere-2026-1366
Preprint. Discussion started: 20 April 2026

by melting pure glacial ice alone. The largest deviations toward higher He concentrations (Fig. 3c) suggest that the glacial meltwater component in Victoria Fjord likely consisted of a mixture of two end-members: 36 % derived from ice that had accumulated crustal He and about 64 % from ice without a crustal He signature. This partitioning highlights the influence of local glacier catchments and bedrock-derived gas fluxes on the noble gas composition of meltwater entering the fjord (Beaird et al., 2015, 2018; Huhn et al., 2021). The coexistence of these contrasting He signatures; crustal He-enriched, low-δ^3He waters near the surface and, AW-influenced, high-δ^3He waters at depth, indicates a vertically structured distribution of freshwater sources, likely reflecting differences in ventilation timescales and mixing pathways within the fjord. The crustal He observed in near-surface waters is consistent with relatively isolated meltwater inputs, potentially originating from submarine melting of icebergs in Victoria Fjord. In contrast, the glacially modified Atlantic-origin layer at depth appeared to remain partially trapped below the mixed layer, rather than rising fully as a buoyant plume as documented in several other Greenland fjords (Mortensen et al., 2020; De Andrés et al., 2020; Cowton et al., 2023). The ^{3}He–^{4}He and ΔNe–ΔHe relationships (Fig. 3b–c) support this dual-origin scenario, revealing (1) atmospheric He addition to subsurface waters and (2) crustal He enrichment within the near-surface layer. Together, these patterns point to distinct meltwater pathways and a vertically differentiated distribution of glacial inputs in Victoria Fjord.

4.3 Water-mass composition and glacial meltwater pathways

We applied a three end-member δ^{18}O–S_A mass balance to estimate the relative contributions of meteoric water (MW) and sea-ice melt (SIM) across the study region. MW and SIM fractions were vertically interpolated at 10 m intervals and integrated from 15 to 200 m depth, thus capturing the main layer influenced by freshwater inputs. Because observations were not available above 15 m, the near-surface freshwater content is not fully constrained; consequently, the integrated inventories should be regarded as lower-bound estimates, particularly in Victoria Fjord, where a shallow mixed layer was observed.

MW inventories showed pronounced spatial variability across the region, ranging from ∼4 to ∼15 m freshwater equivalent, reflecting strong fjord-scale gradients comparable to those reported in other Greenland fjords (e.g., Jackson et al., 2014; Beaird et al., 2018; Mortensen et al., 2020; Muilwijk et al., 2022). Victoria Fjord generally exhibited higher MW inventories than Petermann Fjord (Fig. 4a,c), consistent with differences in fjord–shelf exchange and present sea-ice conditions, as previously observed in the adjacent Sherard Osborn Fjord (Stranne et al., 2021). MW inventories were highest at inner and central stations (reaching ∼14–15 m) and generally decreased toward the fjord entrance, although the highest localized value occurred near a small bay fed by an inland glacier north of Nares Land (Fig. 4a). The lowest MW values (∼4–6 m) occurred at stations located near the fjord entrance. In Petermann Fjord, MW inventories ranged from roughly ∼6 to ∼11 m, with relatively elevated values near the northeastern side of the ice front (Fig. 4c), consistent with the preferential export pathway of glacially modified water along the eastern boundary under cyclonic circulation (Johnson et al., 2011; Heuzé et al., 2017).

The spatial distribution of SIM differed between the two fjords but was predominantly negative across the study region (Fig. 4b,d). In Victoria Fjord, most stations exhibited negative SIM values reaching –2 m freshwater equivalent, indicating that the integrated signal in the upper 200 m reflects brine-enriched waters associated with sea-ice formation rather than net sea-ice melt. This pattern is consistent with the vertical profiles (Supplementary Fig. A2), which show negative or near-zero SIM

https://doi.org/10.5194/egusphere-2026-1366
Preprint. Discussion started: 20 April 2026

fractions across much of the upper water column. Only a limited number of observations showed weakly positive SIM values, in the Lincoln Sea and Victoria Fjord at 50 m depth, suggesting localized melt contributions (Supplementary Fig. A2). In Petermann Fjord, SIM values were consistently negative (–1.5 to –2 m), indicating the presence of waters influenced by winter sea-ice production that persisted into summer, consistent with previously documented seasonal sea-ice cycles in Greenland fjords (Jackson and Straneo, 2016; Stuart-Lee et al., 2021).

The dominance of negative SIM values across the region indicates that freshwater within the upper 200 m was supplied primarily by meteoric sources rather than by sea-ice melt (Supplementary Fig. A2). This signal was particularly strong in Victoria Fjord, where meteoric water inventories were highest, suggesting that glacial input, runoff, and precipitation represented the main freshwater contribution shaping the stratification of the fjord waters. Sea-ice processes appeared to play a secondary role, contributing mainly through brine rejection during formation rather than through meltwater addition. However, part of the SIM signal likely reflects processes that occurred beyond the fjords themselves. In Petermann Fjord, where exchange with the Nares Strait is likely more pronounced, upstream sea-ice formation and the advection of modified water-masses probably influenced the observed freshwater structure. As a result, spatial gradients in freshwater composition provide a clearer picture than absolute values alone. In Victoria Fjord, the accumulation of meteoric freshwater appeared to be largely controlled by local sources, while in Petermann Fjord the freshwater distribution reflected stronger connectivity with shelf waters. In addition, the survey in Petermann Fjord took place later in the season, when the fjord was largely ice free, and part of the SIM signal may therefore represent meltwater advected from the Arctic Ocean through the Nares Strait (Johnson et al., 2011; Heuzé et al., 2017; Shroyer et al., 2017). Generally, these observations suggest that while local melt and sea-ice processes dominated the 15–200 m layer, a minor fraction was linked to larger-scale Arctic freshwater pathways (e.g., Bao and Moffat, 2024).

To resolve the composition of the MW pool, we applied an optimum multiparameter (OMP) analysis to quantify the fractions of subglacial discharge (SGD), submarine meltwater (SMW), and ancient ice melt (AIM), together with Atlantic Water (AW) and Polar Water (PW). In both Victoria and Petermann fjords, deep waters below ∼300 m were dominated by AW, generally exceeding ∼95 % of the water-mass composition (Fig. 5a). This distribution is consistent with the persistent inflow of Atlantic-derived deep waters documented throughout northern Greenland fjords and along the Arctic continental margin (e.g., Jakobsson et al., 2018; Heuzé et al., 2017; Washam et al., 2018; Jakobsson et al., in review). Above this depth, the water column transitions into a layer where PW became the main water-mass between 15 and 100 m (Fig. 5b). Between roughly 100 and 300 m, AW fractions decreased to ∼70–90 % (Fig. 5a), while PW contributed ∼10–30 % (Fig. 5b), with only minor fractions associated with glacial freshwater components (Fig. 5c–d).

Within the upper ∼300 m, glacial meltwater was distributed through a multilayer subsurface structure of SGD (Fig. 5c) and SMW (Fig. 5d), reflecting the subsurface meltwater layer reported in Sermilik Fjord using noble gases (Beaird et al., 2018). In both fjords, SGD represented the dominant meltwater component in the upper water column but decreased rapidly with depth; the highest fractions occurred in the upper ∼100 m and declined to near-zero below 150 m (Fig. 5c). Victoria Fjord exhibited the largest SGD fractions in this layer, reaching 8 %. In contrast, Petermann Fjord showed overall lower fractions, typically remaining below 4 %, indicating weaker local accumulation of subglacial discharge signals relative to Victoria Fjord. In both fjords, SMW occurred at lower concentrations but persisted deeper in the water column than SGD (Fig. 5c–d); generally

https://doi.org/10.5194/egusphere-2026-1366
Preprint. Discussion started: 20 April 2026

on the order of ∼0.8 %, reaching up to 1.4 % within the upper 200 m and remaining detectable at greater depths (Fig. 5d). This vertical distribution suggests that meltwater produced by ice–ocean interactions was transported and mixed below the immediate surface layer, implying that SMW and associated mixing processes influenced depths beyond those affected by buoyant plumes of SGD alone. The contribution of AIM within the SGD and SMW pools further clarifies the origin of the meltwater components. Focusing on the depth range where SMW was most abundant (100–250 m; Fig. 5d), the AIM fraction in the SGD pool (AIM–SGD; Supplementary Fig. A3) was essentially absent, indicating that SGD was primarily derived from relatively young glacial ice delivered through surface melt and the subglacial hydrological system, rather than from meltwater produced from older ice stored deeper within the ice-sheet. In contrast, the AIM fraction in the SMW pool (AIM–SMW; Supplementary Fig. A3) showed greater variability, suggesting that SMW incorporated a larger contribution from older glacial ice exposed at the glacier terminus and along the submerged ice front. This pattern is particularly evident in Victoria Fjord, where a dual AIM structure emerged, with enhanced contributions in a subsurface layer around 150 m and a shallower signal closer to the surface. Such a structure likely reflects multiple pathways of glacially modified water originating from both the main glacier and icebergs, which are known to contribute significantly to freshwater budgets in Greenland fjords (e.g., Enderlin et al., 2016; Moon et al., 2018; Moyer et al., 2019; Davison et al., 2020). This interpretation is consistent with the vertical distributions of δ^3He discussed previously (Fig. 2f), which revealed contrasting signatures between surface and subsurface waters in Victoria Fjord. Differences in plume entrainment dynamics may help explain these patterns (Cowton et al., 2015; Slater et al., 2015). In particular, the relatively limited SMW influence in the upper layer of Petermann Fjord during summer contrasted with the stronger meltwater signals observed in Victoria Fjord, where iceberg melting and enhanced mixing likely promoted upwelling of deeper waters. Overall, the observed distribution aligns with patterns documented in other Greenland fjords (Beaird et al., 2015; Sciascia et al., 2013; Straneo et al., 2011), where glacially modified waters spread throughout the water column rather than being confined to a single layer.

Atmospheric loss of He and Ne was likely minimal in Victoria Fjord due to strong stratification and ice coverage but it might have been more relevant in Petermann Fjord. Despite these differences, meltwater production estimates remained consistent with previous studies (Wilson et al., 2017; Heuzé et al., 2017), supporting the interpretation that SMW pathway was primarily generated below the mixed layer and that associated gas loss does not substantially bias SMW estimates. In Petermann Fjord, the glacially modified layer reached a maximum of ∼1.4 % SMW near 150 m depth, approximately corresponding to the base of the Petermann ice tongue (Heuzé et al., 2017). Using a two-layer fjord circulation framework (Nilsson et al., 2023), together with deep inflow estimates of 0.025–5 Sv (Johnson et al., 2011; Nilsson et al., 2023; Prakash et al., 2025) and a pure meltwater fraction of 0.014, SMW production is estimated at 8–16 Gt yr^{-1} (0.25–0.51 mSv), consistent with earlier estimates (Wilson et al., 2017; Heuzé et al., 2017).

5 Conclusion

This tracer-based analysis provides new insights into the freshwater sources, their distributions, and the associated water-mass structure in Petermann and Victoria fjords. It shows that freshwater in both fjords was dominated by meteoric freshwater input,

https://doi.org/10.5194/egusphere-2026-1366
Preprint. Discussion started: 20 April 2026

largely derived from local glacial melt, with a smaller contribution from non-local Arctic-sourced freshwater advected through the Nares Strait. Elevated ΔHe and ΔNe concentrations identify glacial meltwater below the surface mixed layer in both systems, revealing a coherent subsurface glacially modified water-mass between ∼100 and 250 m depth that was primarily composed of Atlantic waters entrained by subglacial discharge and submarine melting. Taken together, the quantification of water sources in this study and the observed intrusion of warm Atlantic waters into the inner fjord (Jakobsson et al., in review) suggest that the sensitivity of C.H. Ostenfeld Gletsjer is influenced by multiple interacting processes. These include direct subsurface access of warm waters to the glacier terminus, the accumulation of freshwater in surface layers, reduced atmospheric exchanges due to persistent sea-ice cover, and a resulting enhancement in water column stratification. The contrast with Petermann Fjord, where tracer distributions pointed to stronger vertical exchange and more efficient air-sea exchange, highlights the critical role of local fjord conditions in shaping ice–ocean interactions. The combination of fjord geometry, ocean circulation, and freshwater dynamics presented in Jakobsson et al. (in review) and in this study may offer a useful framework for assessing the vulnerability of other outlet glaciers in Greenland. A more detailed understanding of how local physical conditions control tracer distribution and ice–ocean coupling will be essential for improving projections of future ice loss in a rapidly warming Arctic.

https://doi.org/10.5194/egusphere-2026-1366
Preprint. Discussion started: 20 April 2026

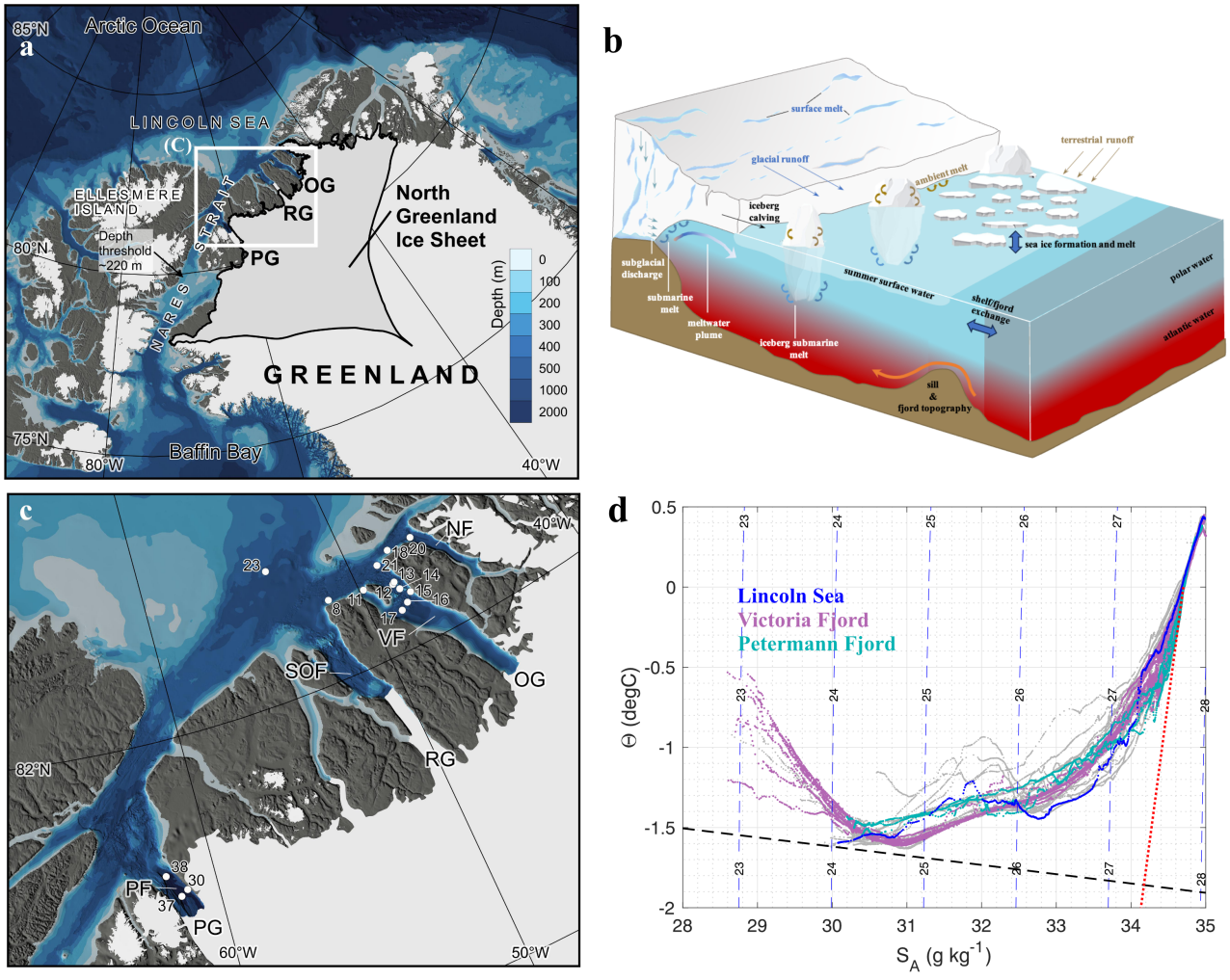

Figure 1. Maps and overview of the study region and hydrographic context. (a) Drainage sectors of the North Greenland Ice Sheet and locations of three marine-terminating glaciers: Petermann Gletsjer (PG), Ryder Gletsjer (RG), and C.H. Ostenfeld Gletsjer (OG). (b) Schematic illustration of a Greenland marine-terminating glacier–fjord system, highlighting key physical processes controlling fjord circulation, interactions at the ice–ocean interface, typical water-mass stratification, and the main sources of freshwater. (c) Map of the study area showing the locations of CTD profiles in the Lincoln Sea and adjacent fjords: Petermann Fjord (PF), Sherard Osborn Fjord (SOF), Victoria Fjord (VF), and Nordenskiöld Fjord (NF). (d) Θ–S_A relationship of CTD data collected during the *GEOEO 2024* (grey). CTD casts associated with noble gas sampling are shown for the Lincoln Sea (blue), Petermann Fjord (green), and Victoria Fjord (purple). The dashed red line indicates the mixing line between ocean water and pure glacial meltwater (the Gade line; Gade, 1979). Bathymetry shown in (a) and (c) is from the International Bathymetric Chart of the Arctic Ocean (IBCAO) version 5.0 (Jakobsson et al., 2024), based on BedMachine v5 in the fjords (Morlighem et al., 2022). Bathymetry in Victoria Fjord has been updated using multibeam data and spot soundings acquired during the *GEOEO 2024* (Jakobsson et al., in review).

https://doi.org/10.5194/egusphere-2026-1366
Preprint. Discussion started: 20 April 2026

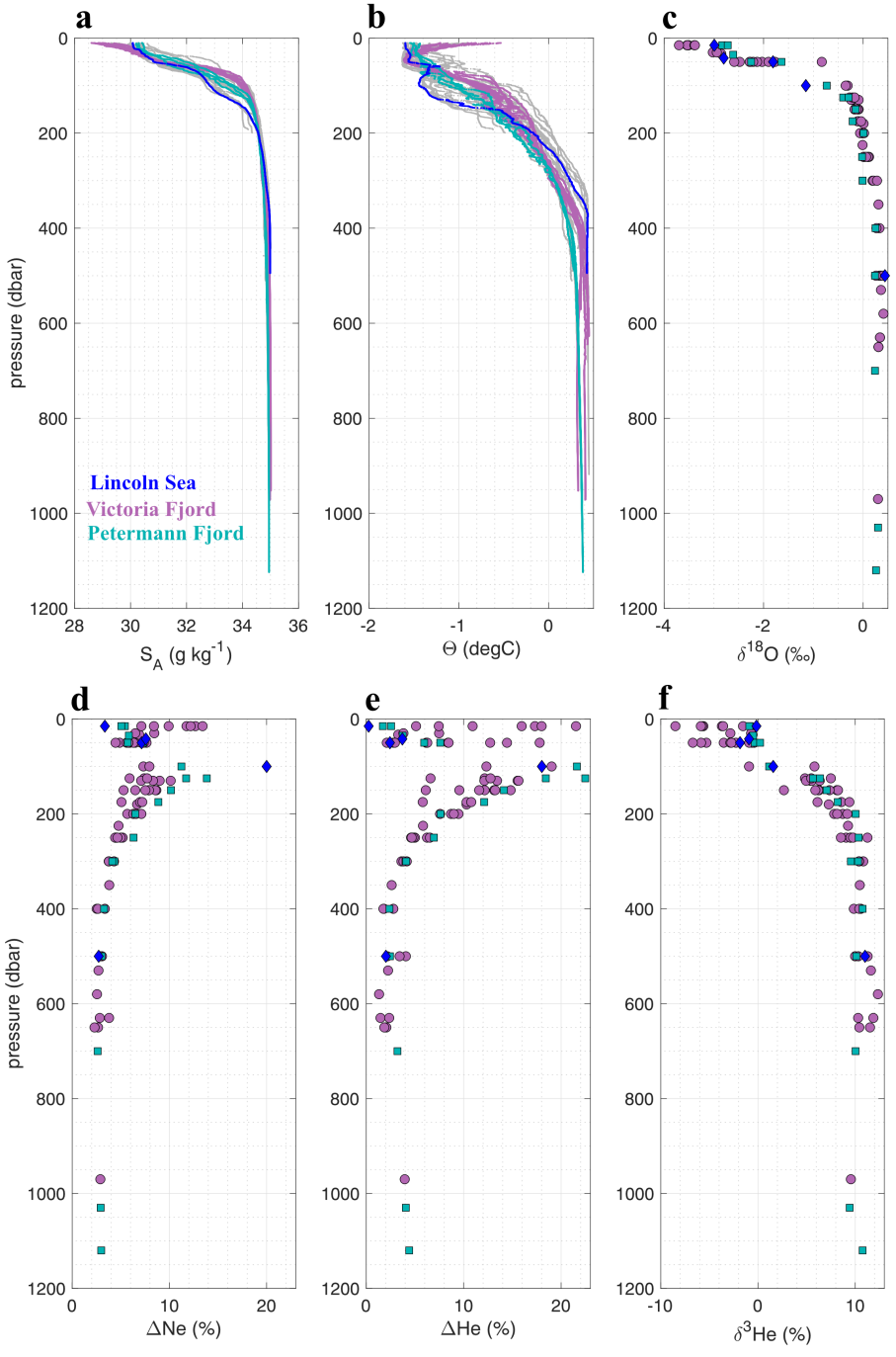

Figure 2. Vertical profiles from CTD stations in the Lincoln Sea, Petermann Fjord, and Victoria Fjord. Profiles of S_A (a), Θ (b), δ^{18}O (c), ΔHe (d), ΔNe (e), and δ^3He (f) are shown. Symbols indicate stations in the Lincoln Sea (blue diamonds), Petermann Fjord (green squares), and Victoria Fjord (purple circles).

https://doi.org/10.5194/egusphere-2026-1366
Preprint. Discussion started: 20 April 2026

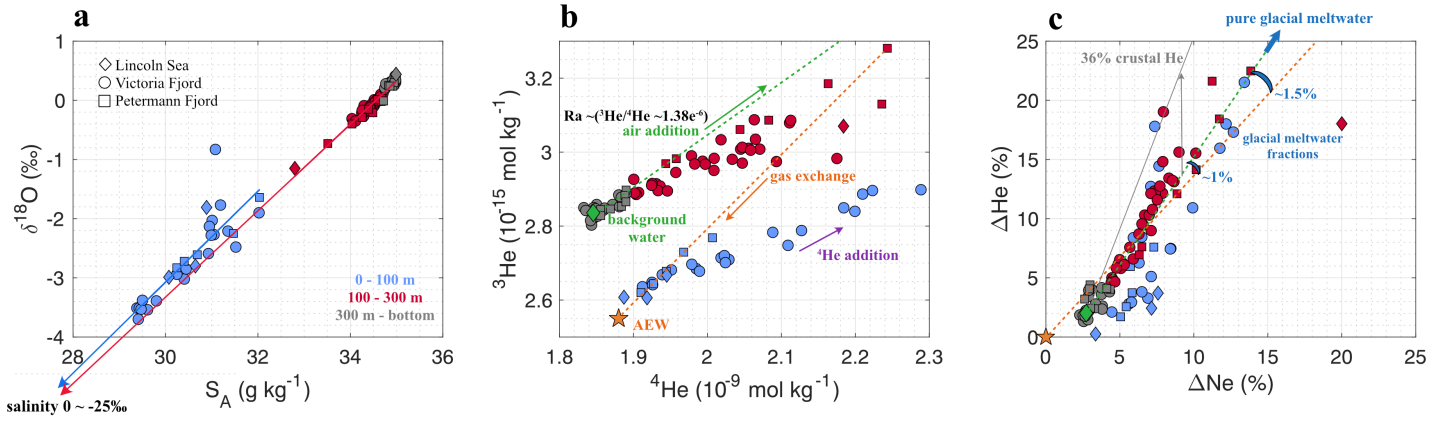

Figure 3. Relationships between hydrographic and tracer properties. (a) δ^{18}O–S_A relationship; the solid blue line shows the regression for observations between 0–100 m, and the solid red line shows the regression for observations between 100–300 m depth. (b) ^{3}He–^{4}He relationship; the dashed green line represents mixing between background water (green diamond) and the atmosphere (slope: 1.38×10^{-6}), and the dashed orange line represents mixing between air-equilibrated water (orange star) and the highest observed He values. (c) ΔHe–ΔNe relationship; the dashed green line indicates mixing between background water and pure (100 %) glacial meltwater. The grey line shows mixing between background water and a mixture of 64 % glacial meltwater and 36 % glacial meltwater with crustal He addition.

https://doi.org/10.5194/egusphere-2026-1366
Preprint. Discussion started: 20 April 2026

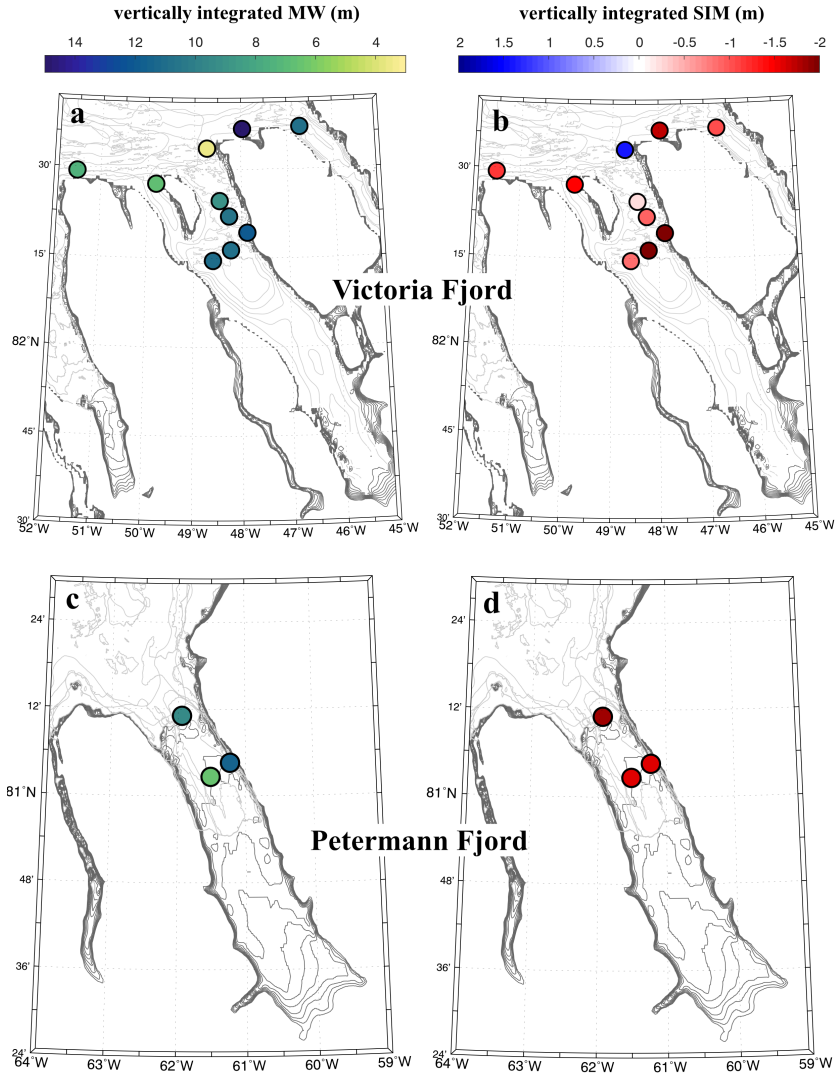

Figure 4. Spatial distribution of meteoric water (MW) and sea-ice melt (SIM) in Petermann and Victoria fjords. Maps show vertically integrated meteoric water content (a–c) and sea-ice melt content (b–d) between 15 and 200 m depth, expressed as equivalent freshwater.

https://doi.org/10.5194/egusphere-2026-1366
Preprint. Discussion started: 20 April 2026

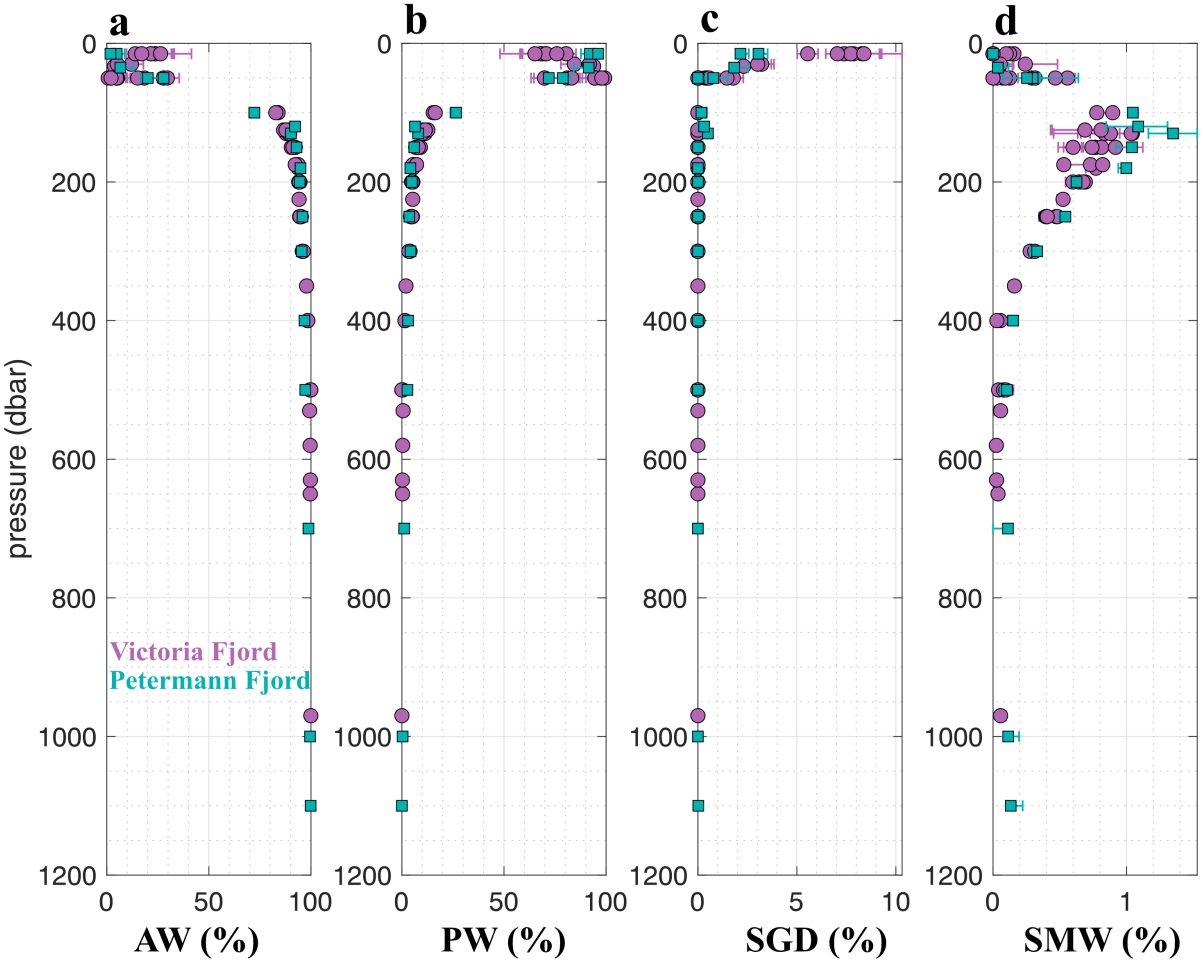

Figure 5. Depth profiles of optimum multiparameter (OMP) fraction solutions for the main water-mass components: Atlantic Water (a), Polar Water (b), subglacial discharge (c), and submarine meltwater (d). Observations from Petermann Fjord are shown in green (squares) and Victoria Fjord in purple (circles). Horizontal error bars indicate the uncertainty derived from perturbed solutions using a Monte Carlo approach (10000 repetitions).

https://doi.org/10.5194/egusphere-2026-1366
Preprint. Discussion started: 20 April 2026

Table 1. End-member properties used in the tracer-based mass balance and OMP analyses. Conservative temperature (Θ), absolute salinity (S_A), δ^{18}O, and noble gas concentrations (^{3}He, Ne, He) are specified for Atlantic Water (AW), Polar Water (PW), subglacial discharge (SGD), submarine meltwater (SMW), and their corresponding contribution of ancient ice melt (AIM).

	Θ (°C)	S_A (g kg^{-1})	δ^{18}O (‰)	^{3}He (10^{-15} mol kg^{-1})	Ne (10^{-9} mol kg^{-1})	He (10^{-9} mol kg^{-1})
AW	0.45	35	0.4	2.84	8.27	1.85
PW	-1.6	31	-2	2.67	9.09	1.92
SGD	0	0	-28	3.001	10.07	2.21
SGD-AIM	0	0	-28	36.2	88.7	33.9
SMW	-87	0	-28	36.2	88.7	26.2
SMW-AIM	-87	0	-28	36.2	88.7	33.9

Table 2. Uncertainties assigned to tracer properties and relative weights used in the tracer-based mass balance and OMP analyses. Following Beaird et al. (2018), the primary source of uncertainty in the noble gas estimates arises from the assumed air content of glacial ice. Therefore, the uncertainties in noble gas concentrations for SGD, SMW, and AIM are taken to be equal to the reported uncertainty in glacial ice air content ($\pm$8 %) from Martinerie et al. (1992).

	Θ (°C)	S_A (g kg^{-1})	δ^{18}O (‰)	^{3}He (10^{-15} mol kg^{-1})	Ne (10^{-9} mol kg^{-1})	He (10^{-9} mol kg^{-1})
AW	0.1	0.1	0.1	0.01	0.04	0.009
PW	0.1	0.1	0.5	0.009	0.03	0.007
SGD	2	0.01	4	0.04	0.2	0.03
SGD-AIM	2	0.01	4	0.04	0.2	0.03
SMW	4	0.01	4	2.69	7.1	2.1
SMW-AIM	4	0.01	4	2.69	7.1	2.1
Weights	104	973	10	33	31	30

https://doi.org/10.5194/egusphere-2026-1366
Preprint. Discussion started: 20 April 2026

Appendix A

https://doi.org/10.5194/egusphere-2026-1366
Preprint. Discussion started: 20 April 2026

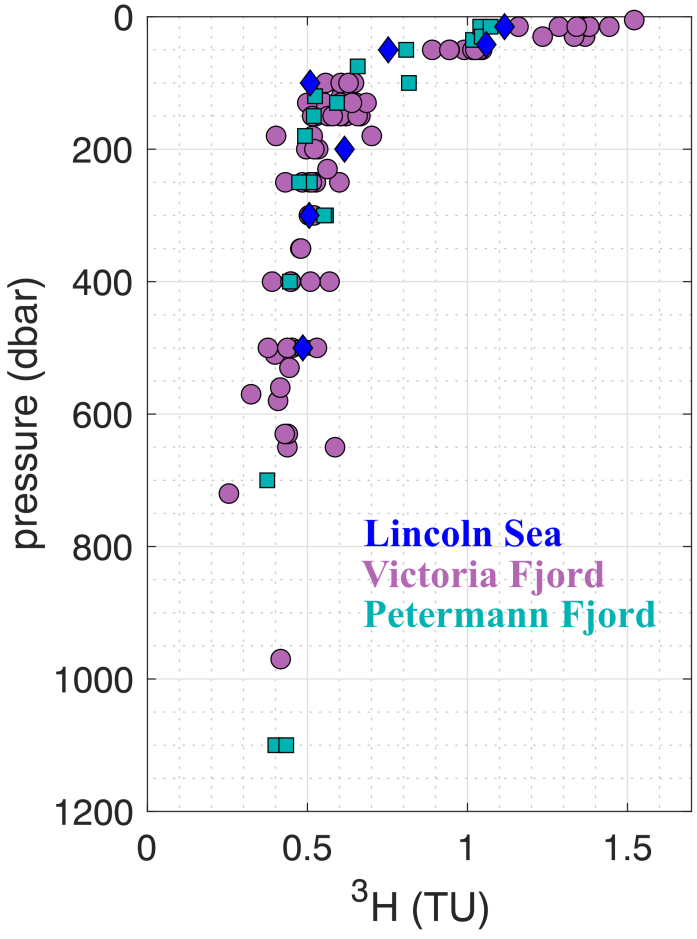

Figure A1. Vertical profiles of ^{3}H from CTD stations in the Lincoln Sea (blue diamonds), Petermann Fjord (green squares), and Victoria Fjord (purple circles).

https://doi.org/10.5194/egusphere-2026-1366
Preprint. Discussion started: 20 April 2026

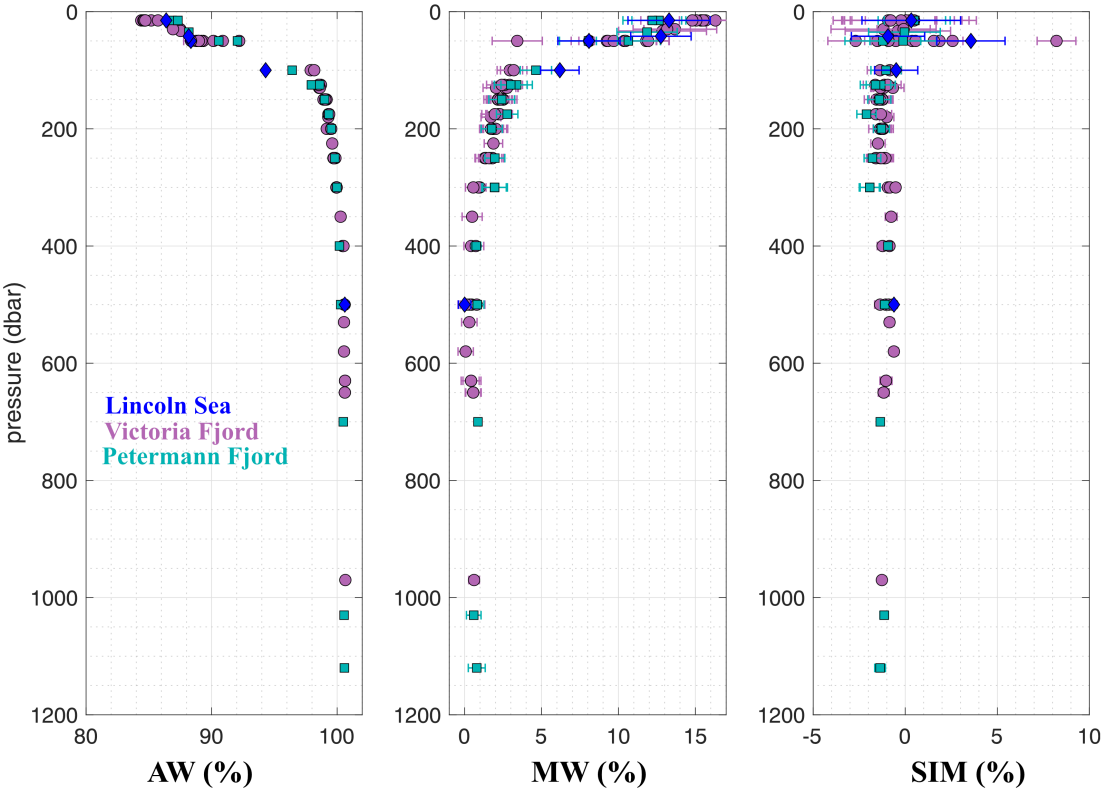

Figure A2. Depth profiles of δ^{18}O–S_A mass-balance fraction solutions for the main water-mass and freshwater components: Atlantic Water (AW), meteoric water (MW), and sea-ice melt (SIM). Observations from Petermann Fjord are shown in green (squares) and Victoria Fjord in purple (circles). Horizontal error bars indicate the uncertainty derived from perturbed solutions using a Monte Carlo approach (10000 repetitions).

https://doi.org/10.5194/egusphere-2026-1366
Preprint. Discussion started: 20 April 2026

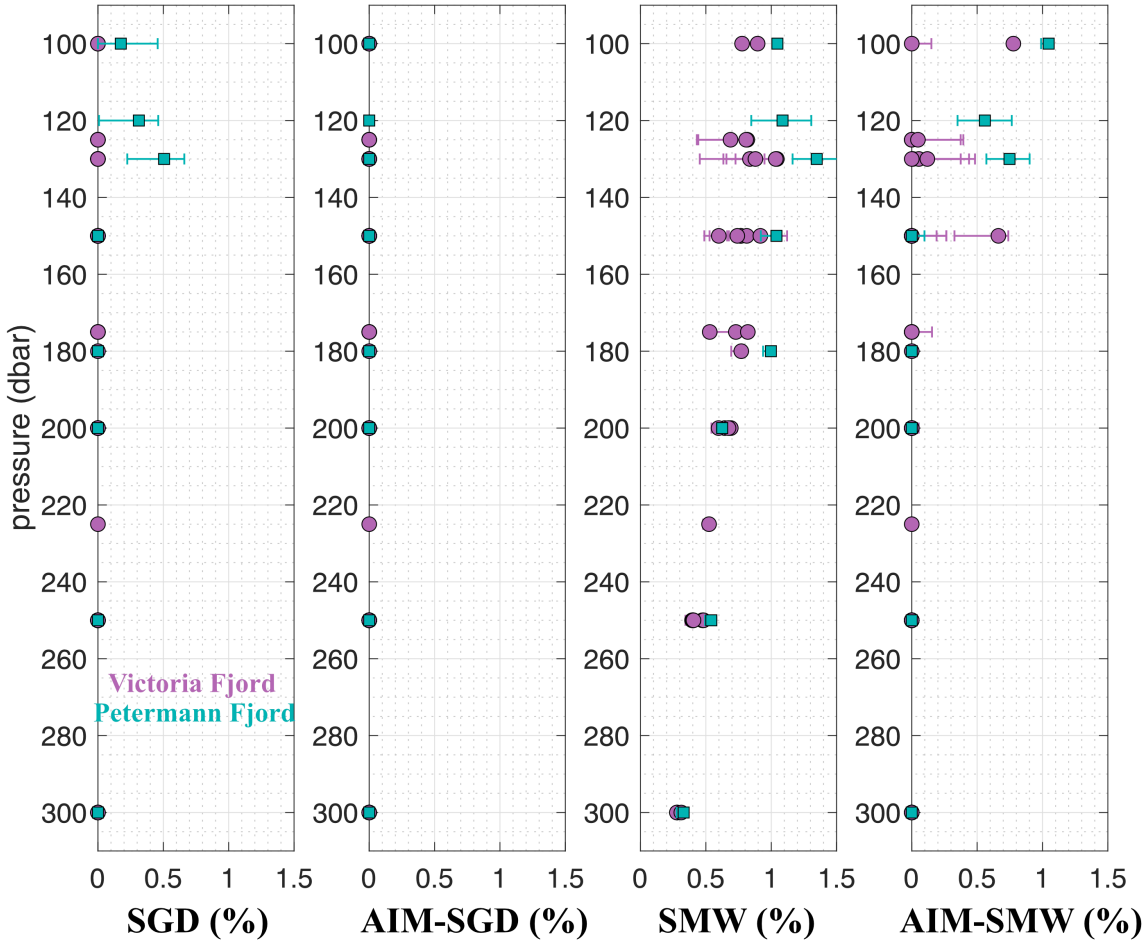

Figure A3. Depth profiles of optimum multiparameter (OMP) fraction solutions between 90 and 350 m depth. Shown are subglacial discharge (SGD), ancient ice melt (AIM) within the SGD pool, submarine meltwater (SMW), and ancient ice melt (AIM) within the SMW pool. Observations from Petermann Fjord are shown in green (squares) and Victoria Fjord in purple (circles). Horizontal error bars indicate the uncertainty derived from perturbed solutions using a Monte Carlo approach (10000 repetitions).

https://doi.org/10.5194/egusphere-2026-1366
Preprint. Discussion started: 20 April 2026

Author contributions. CH.A, C.S. and J.N. conceived the original idea of the paper. C.S., J.N. and W.J. contributed to the data interpretation and to the development of the discussion aspects. J.B., J.S., N.K. and M.J. have contributed to the writing, provided inputs on the manuscript and participated in various ways in the data collection and processing.

Data availability. Oceanographic data acquired during the *GEOEO–North of Greenland 2024 Expedition* and presented in this paper are available in the Bolin Centre for Climate Research Database. https://doi.org/10.17043/oden-geoeo-2024-ctd-1 https://doi.org/10.17043/oden-geoeo-2024-ctd-raw-1

Acknowledgements. The *GEOEO–North of Greenland 2024 Expedition* was conducted as part of the GEOEO (North of Greenland Earth–Ocean–Ecosystem Observatory) research program, endorsed by the Swedish Polar Research Secretariat (SPRS). We sincerely thank the captain and crew of IB *Oden*, as well as the SPRS staff, for their logistical support. CH.A. and M.J. were supported by the Swedish Research Council FORMAS grants 2022-02856_Formas and 2021-01590_Formas, respectively. C.S. was supported by the Swedish Research Council VR grant 2022-04081_VR. M.J. and J.B. were also provided funding from the Swedish Research Council VR grant 2021-04512_VR. IB *Oden* is a Swedish national infrastructure supported by the Swedish Research Council VR grant 2021-00153_VR.

https://doi.org/10.5194/egusphere-2026-1366
Preprint. Discussion started: 20 April 2026

References

Bao, W. and Moffat, C.: Impact of shallow sills on circulation regimes and submarine melting in glacial fjords, The Cryosphere, 18, 187–203, 2024.

Bauch, D., Schlosser, P., and Fairbanks, R. G.: Freshwater balance and the sources of deep and bottom waters in the Arctic Ocean inferred from the distribution of H218O, Progress in Oceanography, 35, 53–80, 1995.

Bauch, D., Erlenkeuser, H., and Andersen, N.: Water mass processes on Arctic shelves as revealed from δ18O of H2O, Global and Planetary Change, 48, 165–174, 2005.

Beaird, N., Straneo, F., and Jenkins, W.: Spreading of Greenland meltwaters in the ocean revealed by noble gases, Geophysical Research Letters, 42, 7705–7713, 2015.

Beaird, N. L., Straneo, F., and Jenkins, W.: Export of strongly diluted Greenland meltwater from a major glacial fjord, Geophysical Research Letters, 45, 4163–4170, 2018.

Benetti, M., Sveinbjörnsdóttir, A., Ólafsdóttir, R., Leng, M. J., Arrowsmith, C., Debondt, K., Fripiat, F., and Aloisi, G.: Inter-comparison of salt effect correction for δ18O and δ2H measurements in seawater by CRDS and IRMS using the gas-H2O equilibration method, Marine Chemistry, 194, 114–123, 2017.

Burgers, T., Miller, L., Rysgaard, S., Mortensen, J., Else, B., Tremblay, J.-É., and Papakyriakou, T.: Distinguishing physical and biological controls on the carbon dynamics in a high-Arctic outlet strait, Journal of Geophysical Research: Oceans, 128, e2022JC019 393, 2023.

Carroll, D., Sutherland, D. A., Shroyer, E. L., Nash, J. D., Catania, G. A., and Stearns, L. A.: Modeling turbulent subglacial meltwater plumes: Implications for fjord-scale buoyancy-driven circulation, Journal of Physical Oceanography, 45, 2169–2185, 2015.

Charette, M. A., Kipp, L. E., Jensen, L. T., Dabrowski, J. S., Whitmore, L. M., Fitzsimmons, J. N., Williford, T., Ulfsbo, A., Jones, E., Bundy, R. M., et al.: The transpolar drift as a source of riverine and shelf-derived trace elements to the central Arctic Ocean, Journal of Geophysical Research: Oceans, 125, e2019JC015 920, 2020.

Clarke, W. B., Jenkins, W., and Top, Z.: Determination of tritium by mass spectrometric measurement of 3He, The international journal of applied radiation and isotopes, 27, 515–522, 1976.

Cottier, F., Nilsen, F., Skogseth, R., Tverberg, V., Skarđhamar, J., and Svendsen, H.: Arctic fjords: a review of the oceanographic environment and dominant physical processes, 2010.

Cowton, T., Slater, D., Sole, A., Goldberg, D., and Nienow, P.: Modeling the impact of glacial runoff on fjord circulation and submarine melt rate using a new subgrid-scale parameterization for glacial plumes, Journal of Geophysical Research: Oceans, 120, 796–812, 2015.

Cowton, T. R., Slater, D. A., and Inall, M. E.: Subglacial-Discharge Plumes Drive Widespread Subsurface Warming in Northwest Greenland's Fjords, Geophysical Research Letters, 50, e2023GL103 801, 2023.

Craig, H. and Scarsi, P.: Helium isotope stratigraphy in the GISP2 ice core, EOS Trans Am Geophys Union, 78, F7, 1997.

Davison, B., Cowton, T., Cottier, F. R., and Sole, A.: Iceberg melting substantially modifies oceanic heat flux towards a major Greenlandic tidewater glacier, Nature communications, 11, 5983, 2020.

De Andrés, E., Slater, D. A., Straneo, F., Otero, J., Das, S., and Navarro, F.: Surface emergence of glacial plumes determined by fjord stratification, The Cryosphere, 14, 1951–1969, 2020.

Dukhovskoy, D. S., Myers, P. G., Platov, G., Timmermans, M.-L., Curry, B., Proshutinsky, A., Bamber, J. L., Chassignet, E., Hu, X., Lee, C. M., et al.: Greenland freshwater pathways in the sub-A rctic S eas from model experiments with passive tracers, Journal of Geophysical Research: Oceans, 121, 877–907, 2016.

https://doi.org/10.5194/egusphere-2026-1366
Preprint. Discussion started: 20 April 2026

Ekwurzel, B., Schlosser, P., Mortlock, R. A., Fairbanks, R. G., and Swift, J. H.: River runoff, sea ice meltwater, and Pacific water distribution and mean residence times in the Arctic Ocean, Journal of Geophysical Research: Oceans, 106, 9075–9092, 2001.

Enderlin, E. M., Howat, I. M., Jeong, S., Noh, M.-J., Van Angelen, J. H., and Van Den Broeke, M. R.: An improved mass budget for the Greenland ice sheet, Geophysical Research Letters, 41, 866–872, 2014.

Enderlin, E. M., Hamilton, G. S., Straneo, F., and Sutherland, D. A.: Iceberg meltwater fluxes dominate the freshwater budget in Greenland's iceberg-congested glacial fjords, Geophysical Research Letters, 43, 11 287–11 294, 2016.

Falkner, K. K., Melling, H., Münchow, A. M., Box, J. E., Wohlleben, T., Johnson, H. L., Gudmandsen, P., Samelson, R., Copland, L., Steffen, K., et al.: Context for the recent massive Petermann Glacier calving event, Eos, Transactions American Geophysical Union, 92, 117–118, 2011.

Fraser, N. J., Skogseth, R., Nilsen, F., and Inall, M. E.: Circulation and exchange in a broad Arctic fjord using glider-based observations, Polar research, 37, 1485 417, 2018.

Gjelstrup, C. V., Sejr, M. K., de Steur, L., Christiansen, J. S., Granskog, M. A., Koch, B. P., Møller, E. F., Winding, M. H., and Stedmon, C. A.: Vertical redistribution of principle water masses on the Northeast Greenland Shelf, Nature Communications, 13, 7660, 2022.

Greve, R. and Chambers, C.: Mass loss of the Greenland ice sheet until the year 3000 under a sustained late-21st-century climate, Journal of Glaciology, 68, 618–624, 2022.

Hahm, D., Postlethwaite, C. F., Tamaki, K., and Kim, K.-R.: Mechanisms controlling the distribution of helium and neon in the Arctic seas: The case of the Knipovich Ridge, Earth and Planetary Science Letters, 229, 125–139, 2004.

Heuzé, C., Wåhlin, A., Johnson, H. L., and Münchow, A.: Pathways of meltwater export from Petermann Glacier, Greenland, Journal of Physical Oceanography, 47, 405–418, 2017.

Hill, E. A., Carr, J. R., and Stokes, C. R.: A review of recent changes in major marine-terminating outlet glaciers in Northern Greenland, Frontiers in Earth Science, 4, 111, 2017.

Hohmann, R., Schlosser, P., Jacobs, S., Ludin, A., and Weppernig, R.: Excess helium and neon in the southeast Pacific: Tracers for glacial meltwater, Journal of Geophysical Research: Oceans, 107, 19–1, 2002.

Huhn, O., Hellmer, H. H., Rhein, M., Rodehacke, C., Roether, W., Schodlok, M. P., and Schröder, M.: Evidence of deep-and bottom-water formation in the western Weddell Sea, Deep Sea Research Part II: Topical Studies in Oceanography, 55, 1098–1116, 2008.

Huhn, O., Rhein, M., Kanzow, T., Schaffer, J., and Sültenfuß, J.: Submarine meltwater from Nioghalvfjerdsbræ (79 north Glacier), northeast Greenland, Journal of Geophysical Research: Oceans, 126, e2021JC017 224, 2021.

Jackson, J. M., Lique, C., Alkire, M., Steele, M., Lee, C. M., Smethie, W. M., and Schlosser, P.: On the waters upstream of Nares Strait, Arctic Ocean, from 1991 to 2012, Continental Shelf Research, 73, 83–96, 2014.

Jackson, R. H. and Straneo, F.: Heat, salt, and freshwater budgets for a glacial fjord in Greenland, Journal of Physical Oceanography, 46, 2735–2768, 2016.

Jakobsson, M., Hogan, K. A., Mayer, L. A., Mix, A., Jennings, A., Stoner, J., Eriksson, B., Jerram, K., Mohammad, R., Pearce, C., et al.: The Holocene retreat dynamics and stability of Petermann Glacier in northwest Greenland, Nature communications, 9, 2104, 2018.

Jakobsson, M., Mayer, L. A., Nilsson, J., Stranne, C., Calder, B., O'Regan, M., Farrell, J. W., Cronin, T. M., Brüchert, V., Chawarski, J., et al.: Ryder Glacier in northwest Greenland is shielded from warm Atlantic water by a bathymetric sill, Communications Earth & Environment, 1, 45, 2020.

Jakobsson, M., Mohammad, R., Karlsson, M., Salas-Romero, S., Vacek, F., Heinze, F., Bringensparr, C., Castro, C. F., Johnson, P., Kinney, J., et al.: The international bathymetric chart of the arctic ocean version 5.0, Scientific data, 11, 1420, 2024.

https://doi.org/10.5194/egusphere-2026-1366
Preprint. Discussion started: 20 April 2026

Jakobsson, M., Kirchner, N., Nilsson, J., Stranne, C., Mayer, L., Barnett, J., Holmes, F., et al.: The Role of Atlantic Water in the Break-up of C.H. Ostenfeld Glacier's Ice Tongue, Northwest Greenland, Communications Earth & Environment, in review.

Jean-Baptiste, P., Petit, J.-R., Lipenkov, V. Y., Raynaud, D., and Barkov, N. I.: Constraints on hydrothermal processes and water exchange in Lake Vostok from helium isotopes, Nature, 411, 460–462, 2001.

Jenkins, A.: Convection-driven melting near the grounding lines of ice shelves and tidewater glaciers, Journal of Physical Oceanography, 41, 2279–2294, 2011.

Jenkins, W., Lott III, D., and Cahill, K.: A determination of atmospheric helium, neon, argon, krypton, and xenon solubility concentrations in water and seawater, Marine Chemistry, 211, 94–107, 2019.

Johnson, H., Münchow, A., Falkner, K., and Melling, H.: Ocean circulation and properties in Petermann Fjord, Greenland, Journal of Geophysical Research: Oceans, 116, 2011.

Kopec, B. G., Klein, E. S., Feldman, G. C., Pedron, S. A., Bailey, H., Causey, D., Hubbard, A., Marttila, H., and Welker, J. M.: Arctic freshwater sources and ocean mixing relationships revealed with seawater isotopic tracing, Journal of Geophysical Research: Oceans, 129, e2023JC020 583, 2024.

Loose, B. and Jenkins, W.: The five stable noble gases are sensitive unambiguous tracers of glacial meltwater, Geophysical Research Letters, 41, 2835–2841, 2014.

Loose, B., Schlosser, P., Smethie, W., and Jacobs, S.: An optimized estimate of glacial melt from the Ross Ice Shelf using noble gases, stable isotopes, and CFC transient tracers, Journal of Geophysical Research: Oceans, 114, 2009.

Martinerie, P., Raynaud, D., Etheridge, D. M., Barnola, J.-M., and Mazaudier, D.: Physical and climatic parameters which influence the air content in polar ice, Earth and Planetary Science Letters, 112, 1–13, 1992.

Masson-Delmotte, V., Hou, S., Ekaykin, A., Jouzel, J., Aristarain, A., Bernardo, R., Bromwich, D., Cattani, O., Delmotte, M., Falourd, S., et al.: A review of Antarctic surface snow isotopic composition: Observations, atmospheric circulation, and isotopic modeling, Journal of climate, 21, 3359–3387, 2008.

Millan, R., Jager, E., Mouginot, J., Wood, M., Larsen, S., Mathiot, P., Jourdain, N., and Bjørk, A.: Rapid disintegration and weakening of ice shelves in North Greenland, Nature Communications, 14, 6914, 2023.

Monteban, D., Pedersen, J. O. P., and Nielsen, M. H.: Physical oceanographic conditions and a sensitivity study on meltwater runoff in a West Greenland fjord: Kangerlussuaq, Oceanologia, 62, 460–477, 2020.

Moon, T., Sutherland, D., Carroll, D., Felikson, D., Kehrl, L., and Straneo, F.: Subsurface iceberg melt key to Greenland fjord freshwater budget, Nature Geoscience, 11, 49–54, 2018.

Moore, G., Schweiger, A., Zhang, J., and Steele, M.: Spatiotemporal variability of sea ice in the Arctic's last ice area, Geophysical Research Letters, 46, 11 237–11 243, 2019.

Moore, G., Howell, S., and Brady, M.: Evolving relationship of Nares Strait ice arches on sea ice along the Strait and the North Water, the Arctic's most productive polynya, Scientific Reports, 13, 9809, 2023.

Morlighem, M., ..., ..., and ...: IceBridge BedMachine Greenland, Version 5, https://doi.org/10.5067/GMEVBWFLWA7X, 2022.

Mortensen, J., Rysgaard, S., Bendtsen, J., Lennert, K., Kanzow, T., Lund, H., and Meire, L.: Subglacial discharge and its down-fjord transformation in West Greenland fjords with an ice mélange, Journal of Geophysical Research: Oceans, 125, e2020JC016 301, 2020.

Mouginot, J., Rignot, E., Bjørk, A. A., Van den Broeke, M., Millan, R., Morlighem, M., Noël, B., Scheuchl, B., and Wood, M.: Forty-six years of Greenland Ice Sheet mass balance from 1972 to 2018, Proceedings of the national academy of sciences, 116, 9239–9244, 2019.

https://doi.org/10.5194/egusphere-2026-1366
Preprint. Discussion started: 20 April 2026

Moyer, A., Sutherland, D., Nienow, P., and Sole, A.: Seasonal variations in iceberg freshwater flux in Sermilik Fjord, southeast Greenland from Sentinel-2 imagery, Geophysical Research Letters, 46, 8903–8912, 2019.

Muilwijk, M., Straneo, F., Slater, D. A., Smedsrud, L. H., Holte, J., Wood, M., Andresen, C. S., and Harden, B.: Export of ice sheet meltwater from Upernavik Fjord, West Greenland, Journal of Physical Oceanography, 52, 363–382, 2022.

Münchow, A.: Volume and freshwater flux observations from Nares Strait to the west of Greenland at daily time scales from 2003 to 2009, Journal of Physical Oceanography, 46, 141–157, 2016.

Münchow, A., Padman, L., and Fricker, H. A.: Interannual changes of the floating ice shelf of Petermann Gletscher, North Greenland, from 2000 to 2012, Journal of Glaciology, 60, 489–499, 2014.

Nilsson, J., van Dongen, E., Jakobsson, M., O'Regan, M., and Stranne, C.: Hydraulic suppression of basal glacier melt in sill fjords, The Cryosphere, 17, 2455–2476, 2023.

Östlund, H. G. and Hut, G.: Arctic Ocean water mass balance from isotope data, Journal of Geophysical Research: Oceans, 89, 6373–6381, 1984.

Otosaka, I. N., Shepherd, A., Ivins, E. R., Schlegel, N.-J., Amory, C., van den Broeke, M., Horwath, M., Joughin, I., King, M., Krinner, G., et al.: Mass balance of the Greenland and Antarctic ice sheets from 1992 to 2020, Earth System Science Data Discussions, 2022, 1–33, 2022.

Pasqualini, A., Schlosser, P., Newton, R., Smethie Jr, W., and Friedrich, R.: A multi-decade tracer study of the circulation and spreading rates of Atlantic water in the Arctic Ocean, Journal of Geophysical Research: Oceans, 129, e2023JC020 738, 2024.

Pattyn, F., Ritz, C., Hanna, E., Asay-Davis, X., DeConto, R., Durand, G., Favier, L., Fettweis, X., Goelzer, H., Golledge, N. R., et al.: The Greenland and Antarctic ice sheets under 1.5 C global warming, Nature climate change, 8, 1053–1061, 2018.

Prakash, A., Zhou, Q., Hattermann, T., and Kirchner, N.: Enhanced subglacial discharge amplifies Petermann Ice Shelf melting when ocean thermal forcing saturates, Nature Communications, 16, 4213, 2025.

Rhein, M., Steinfeldt, R., Huhn, O., Sültenfuß, J., and Breckenfelder, T.: Greenland submarine melt water observed in the Labrador and Irminger Sea, Geophysical Research Letters, 45, 10–570, 2018.

Rysgaard, S., Mortensen, J., Haxen, M., Gillard, L., and Risgaard-Petersen, N.: Summer hydrography conditions at proglacial fjord entrances along East Greenland, Journal of Geophysical Research: Oceans, 129, e2023JC020 665, 2024.

Schaffer, J., Kanzow, T., von Appen, W.-J., von Albedyll, L., Arndt, J. E., and Roberts, D. H.: Bathymetry constrains ocean heat supply to Greenland's largest glacier tongue, Nature Geoscience, 13, 227–231, 2020.

Schlosser, P.: Helium: a new tracer in Antarctic oceanography, Nature, 321, 233–235, 1986.

Sciascia, R., Straneo, F., Cenedese, C., and Heimbach, P.: Seasonal variability of submarine melt rate and circulation in an East Greenland fjord, Journal of Geophysical Research: Oceans, 118, 2492–2506, 2013.

Shroyer, E. L., Padman, L., Samelson, R., Münchow, A., and Stearns, L. A.: Seasonal control of Petermann Gletscher ice-shelf melt by the ocean's response to sea-ice cover in Nares Strait, Journal of Glaciology, 63, 324–330, 2017.

Slater, D. and Straneo, F.: Submarine melting of glaciers in Greenland amplified by atmospheric warming, Nature Geoscience, 15, 794–799, 2022.

Slater, D., Nienow, P., Cowton, T., Goldberg, D., and Sole, A.: Effect of near-terminus subglacial hydrology on tidewater glacier submarine melt rates, Geophysical Research Letters, 42, 2861–2868, 2015.

Song, D., Newton, R., Schlosser, P., and Pfirman, S.: Stable isotope δ18O dynamic fractionation coefficient between water and sea ice in the Arctic Ocean, Journal of Glaciology, 71, e59, 2025.

https://doi.org/10.5194/egusphere-2026-1366
Preprint. Discussion started: 20 April 2026

Straneo, F. and Cenedese, C.: The dynamics of Greenland's glacial fjords and their role in climate, Annual review of marine science, 7, 89–112, 2015.

Straneo, F., Curry, R. G., Sutherland, D. A., Hamilton, G. S., Cenedese, C., Våge, K., and Stearns, L. A.: Impact of fjord dynamics and glacial runoff on the circulation near Helheim Glacier, Nature Geoscience, 4, 322–327, 2011.

Stranne, C., Nilsson, J., Ulfsbo, A., O'Regan, M., Coxall, H. K., Meire, L., Muchowski, J., Mayer, L. A., Brüchert, V., Fredriksson, J., et al.: The climate sensitivity of northern Greenland fjords is amplified through sea-ice damming, Communications Earth & Environment, 2, 70, 2021.

Stuart-Lee, A., Mortensen, J., Kaaden, A.-S. v. d., and Meire, L.: Seasonal hydrography of Ameralik: a southwest Greenland fjord impacted by a land-terminating glacier, Journal of Geophysical Research: Oceans, 126, e2021JC017 552, 2021.

Sültenfuß, J., Roether, W., and Rhein, M.: The Bremen mass spectrometric facility for the measurement of helium isotopes, neon, and tritium in water, Isotopes in Environmental and Health Studies, 45, 83–95, 2009.

Sutherland, D. A., Straneo, F., and Pickart, R. S.: Characteristics and dynamics of two major Greenland glacial fjords, Journal of Geophysical Research: Oceans, 119, 3767–3791, 2014.

Tomczak, M. and Large, D. G.: Optimum multiparameter analysis of mixing in the thermocline of the eastern Indian Ocean, Journal of Geophysical Research: Oceans, 94, 16 141–16 149, 1989.

Vries, A. L., van de Berg, W. J., Noël, B., Meire, L., and van den Broeke, M. R.: Seasonal and interannual variability in freshwater sources for Greenland's fjords, The Cryosphere, 19, 3897–3914, 2025.

Washam, P., Münchow, A., and Nicholls, K. W.: A decade of ocean changes impacting the ice shelf of Petermann Gletscher, Greenland, Journal of Physical Oceanography, 48, 2477–2493, 2018.

Weiss, R., Östlund, H., and Craig, H.: Geochemical studies of the Weddell Sea, Deep Sea Research Part A. Oceanographic Research Papers, 26, 1093–1120, 1979.

Wekerle, C., McPherson, R., von Appen, W.-J., Wang, Q., Timmermann, R., Scholz, P., Danilov, S., Shu, Q., and Kanzow, T.: Atlantic Water warming increases melt below Northeast Greenland's last floating ice tongue, Nature Communications, 15, 1336, 2024.

Wilson, N., Straneo, F., and Heimbach, P.: Satellite-derived submarine melt rates and mass balance (2011–2015) for Greenland's largest remaining ice tongues, The Cryosphere, 11, 2773–2782, 2017.

Wiskandt, J., Nilsson, J., and Koszalka, I. M.: Hydraulic control of submarine glacial melt in Greenlandic fjords, Journal of Geophysical Research: Oceans, 130, e2024JC021 257, 2025.

Yamamoto-Kawai, M., Tanaka, N., and Pivovarov, S.: Freshwater and brine behaviors in the Arctic Ocean deduced from historical data of δ18O and alkalinity (1929–2002 AD), Journal of Geophysical Research: Oceans, 110, 2005.